Reentrant Phase Diagram of $Yb_2Ti_2O_7$ in a $\langle 111 \rangle$ Magnetic Field

A. Scheie,[1,2] J. Kindervater,[1,2] S. Säubert,[3,4] C. Duvinage,[3] C. Pfleiderer,[3] H. J. Changlani,[1,2] S. Zhang,[1,2]
L. Harriger,[5] K. Arpino,[6,2] S. M. Koohpayeh,[1,2] O. Tchernyshyov,[1,2] and C. Broholm[1,2,5,7]

[1]*Department of Physics and Astronomy, Johns Hopkins University, Baltimore, Maryland 21218, USA*
[2]*Institute for Quantum Matter, Johns Hopkins University, Baltimore, Maryland 21218, USA*
[3]*Physik-Department, Technische Universität München, D-85748 Garching, Germany*
[4]*Heinz Maier-Leibnitz Zentrum, Technische Universität München, D-85748 Garching, Germany*
[5]*NIST Center for Neutron Research, National Institute of Standards and Technology, Gaithersburg, Maryland 20899, USA*
[6]*Department of Chemistry, Johns Hopkins University, Baltimore, Maryland 21218, USA*
[7]*Department of Materials Science and Engineering, Johns Hopkins University, Baltimore, Maryland 21218, USA*

We present a magnetic phase diagram of rare-earth pyrochlore $Yb_2Ti_2O_7$ in a $\langle 111 \rangle$ magnetic field. Using heat capacity, magnetization, and neutron scattering data, we show an unusual field dependence of a first-order phase boundary, wherein a small applied field increases the ordering temperature. The zero-field ground state has ferromagnetic domains, while the spins polarize along $\langle 111 \rangle$ above 0.65 T. A classical Monte Carlo analysis of published Hamiltonians does account for the critical field in the low T limit. However, this analysis fails to account for the large bulge in the reentrant phase diagram, suggesting that either long-range interactions or quantum fluctuations govern low field properties.

$Yb_2Ti_2O_7$ may be one of the most famous materials in frustrated magnetism, and yet its ground state has not been fully established. Yb^{3+} ions, each forming a Kramers doublet, occupy the vertices of a (pyrochlore) lattice of corner-sharing tetrahedra which frustrates the development of conventional long range order [1–3]. Much of the recent attention to $Yb_2Ti_2O_7$ has been driven by the suggestion that this material forms a quantum spin ice at low temperatures [4–8], wherein the spins are constrained to point into or out of tetrahedra with a two-in-two-out "ice rule." This exotic state of matter is predicted to have a spin-liquid ground state with its own effective field theory [9,10]. The quantum spin ice (QSI) hypothesis is supported by evidence of monopoles in the paramagnetic phase [6–8], and diffuse zero-field inelastic neutron scattering [11,12]. Challenging the QSI hypothesis, however, is evidence that stoichiometric $Yb_2Ti_2O_7$ ferromagnetically orders around 270 mK (though the specific ordered structure is contested) [11,13,14] with magnetic order enhanced under pressure [15]. It is unclear how to reconcile the ground state order of $Yb_2Ti_2O_7$ with its more unusual behavior, especially since the ground state is not fully understood. What is more, there is limited experimental information about collective properties of $Yb_2Ti_2O_7$ due to the lack of stoichiometrically pure crystals.

Here we report the phase diagram of stoichiometric $Yb_2Ti_2O_7$ in a $\langle 111 \rangle$ magnetic field. The $\langle 111 \rangle$ field in pyrochlore compounds like $Yb_2Ti_2O_7$ harbors the possibility of a quantum kagome ice phase [16], but our data do not reveal such a phase in $Yb_2Ti_2O_7$. Instead, we find a reentrant phase diagram where magnetic order is enhanced under small magnetic fields—a behavior that extant models

of $Yb_2Ti_2O_7$ fail to explain when quantum fluctuations are neglected.

An unfortunate obstacle to studying $Yb_2Ti_2O_7$ is that most single crystals are plagued by site disordered "stuffing," which causes large variations in the critical temperature [17–21]. This extreme sensitivity to disorder makes it difficult to compare experimental results to each other or to theory. Recently, however, high-quality stoichiometric single crystals were successfully grown with the traveling solvent floating zone method [22]. We report the first field-dependent measurements on stoichiometric single crystals of $Yb_2Ti_2O_7$, and we use them to build a phase diagram of $Yb_2Ti_2O_7$ in a $\langle 111 \rangle$ magnetic field. In our analysis, we used three experimental methods: heat capacity, magnetization, and neutron scattering.

The heat capacity of $Yb_2Ti_2O_7$ at various magnetic fields is shown in Fig. 1. We collected heat capacity data on a 1.04 mg sample of $Yb_2Ti_2O_7$ in a $\langle 111 \rangle$ oriented magnetic field using a dilution unit insert of a Quantum Design PPMS [23]. The heat capacity data were collected mostly with a long-pulse method, in which we applied a long heat pulse, tracked sample temperature as the sample cooled, and computed heat capacity from the time derivative of sample temperature (see Ref. [24] and Supplemental Material [25] for more details). The advantage of the long-pulse method is sensitivity to first order transitions, which $Yb_2Ti_2O_7$ is reported to have [26–28]. Some adiabatic short-pulse data were taken as well, and Fig. 1 shows the overall agreement between these two methods.

The magnetic fields in Fig. 1(b) have been corrected for the internal demagnetizing field. The demagnetization correction (see inset) is $H_{int} = H_{ext} - DM(H_{int})$, where D is

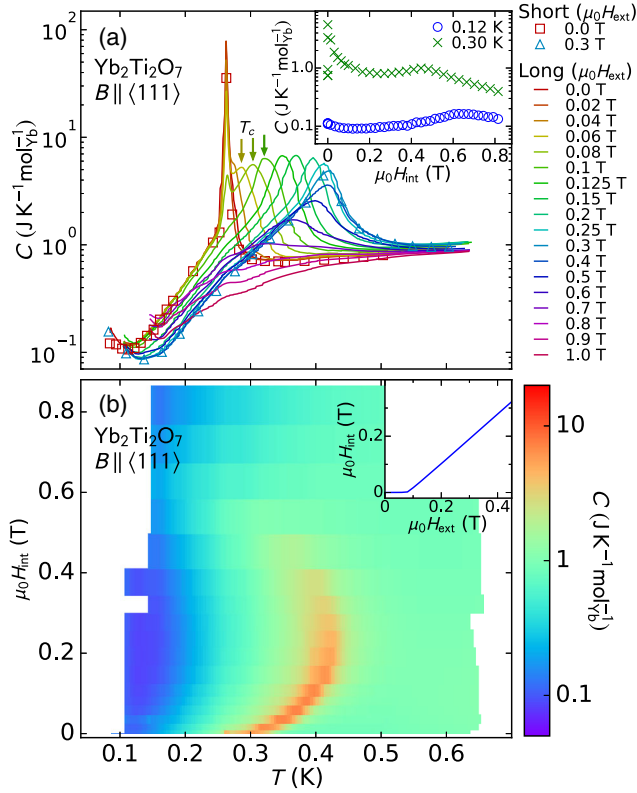FIG. 1.   Heat capacity data for $Yb_2Ti_2O_7$ with magnetic field along $\langle 111 \rangle$. (a) C vs T at various fields. Solid traces indicate long-pulse data, while discrete symbols indicate adiabatic short-pulse data. The fields in the legend are external fields. [(a), inset] Isothermal field scans of heat capacity using the short-pulse method. (b) Color map of long-pulse heat capacity data vs temperature and internal magnetic field. [(b), inset] Relationship between $\mu_0 H_{int}$ and $\mu_0 H_{ext}$.

the demagnetization factor (determined by sample geometry) [29], and $M(H_{int})$ is magnetization (measured separately; see below). This correction enables quantitative comparison between measurements on differently shaped samples.

The magnetization of $Yb_2Ti_2O_7$ (Fig. 2) was measured by means of a bespoke vibrating coil magnetometer (VCM) as combined with a TL400 Oxford Instruments top-loading dilution refrigerator [23,30–33]. We measured the temperature dependence of the magnetization while cooling and while heating, with field-heating measurements performed on both a zero-field-cooled and a field-cooled state. Similarly, we measured field dependence magnetization with field sweeps from $0 \rightarrow 1$ T performed on a zero-field-cooled sample, followed by field sweeps from $+1$ T $\rightarrow -1$ T and -1 T $\rightarrow +1$ T. Further details are provided in the Supplemental Material [25]. All magnetization measurements were carried out on a 4.7 mm diameter, 0.40 g sphere of $Yb_2Ti_2O_7$, which was ground from a larger stoichiometric single crystal and polished into a spherical shape. The spherical geometry ensures a uniform demagnetization factor of $D = 1/3$.

Finally, we collected neutron diffraction data at the SPINS cold neutron triple axis spectrometer at the NCNR. Our sample for these experiments was a 4.7 mm $Yb_2Ti_2O_7$ sphere (ground from the same crystal as the magnetization sample) in a dilution refrigerator with the $\langle 111 \rangle$ direction perpendicular to the scattering plane and along a vertical magnetic field, with $E_i = E_f = 5$ meV neutrons and a full width at half maximum incoherent elastic energy resolution of 0.23 meV [34]. To explore the phase boundaries seen in the heat capacity and magnetization measurements, we focused our attention on the $(2\bar{2}0)$ peak, which was reported to be magnetic [11,14]. We first allowed the sample to settle into the ground state at zero field by cooling from 300 K over 17 h and allowing the sample to sit for an additional 7 h at
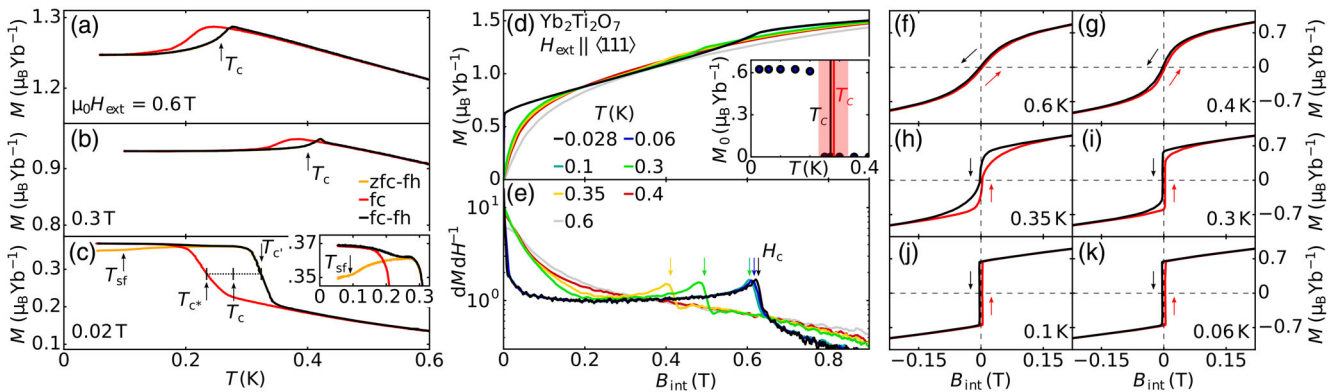

FIG. 2.   Magnetization of $Yb_2Ti_2O_7$ in applied magnetic fields along $\langle 111 \rangle$. (a)–(c) Temperature dependence of the magnetization where we distinguish between data recorded according to procedure (i) zero-field-cooled or field-heated (zfc-fh), (ii) field-cooled (fc), and (iii) field-cooled or field-heated (fc-fh). (d) Magnetization and (e) numerical derivative of the experimental data of $Yb_2Ti_2O_7$ as a function of internal magnetic field after correction for demagnetization fields. The inset in (d) shows the spontaneous magnetization as a function of temperature obtained from magnetization field sweeps [protocol (A1); see the Supplemental Material [25]]. (f)–(k) Magnetization in field cycles of sweep types protocol (A2) and (A3) (see Supplemental Material [25]).

65 mK. Following this, we scanned the applied magnetic field at 100 mK from 0 to 1 T, and then performed slow temperature scans at various fields. The results are shown in Fig. 3. The neutron scattering measurements were taken with the detector sitting at the $(2\bar{2}0)$ Bragg peak's maximum intensity, with periodic rocking scans to ensure alignment after cryogenic operations.

All three methods—heat capacity, magnetization, and neutron diffraction—point to a reentrant phase diagram of $Yb_2Ti_2O_7$ in a $\langle 111 \rangle$ magnetic field. The heat capacity plot in Fig. 1 presents the clearest manifestation. At zero field, $C(T)$ has a sharp peak at 270 mK, as reported for stoichiometric powders [18,22], indicating a phase transition. A magnetic field initially causes this phase boundary to shift up in temperature, reaching a maximum temperature of 0.42 K at an internal field of 0.24 T. At higher fields, the phase boundary sweeps back to 0 K at 0.65 T. The data in Fig. 1(a) show two heat capacity peaks at fields between 0.02 and 0.1 T. This is consistent with the result of field inhomogeneity from nonuniform demagnetizing fields in the
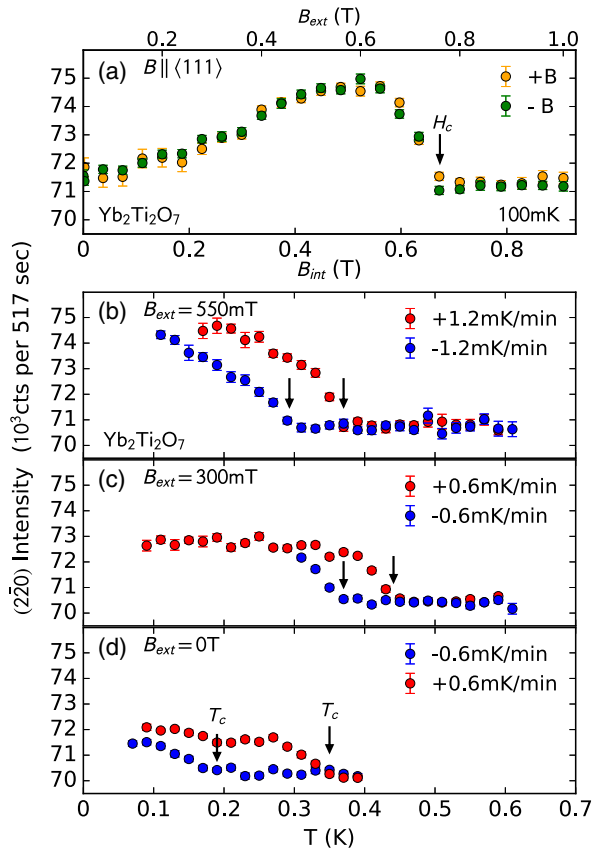
platelike specific heat sample. In a weak external field (below 0.1 T), the center of the sample still has no net internal field, giving rise to a residual sharp peak with the same T_c as in zero external field. The residual peak disappears as soon as the entire sample has a nonzero net field. This field inhomogeneity would also broaden the peak in finite fields (see Supplemental Material [25] for more details).

The magnetization data in Fig. 2 contain several important features. First, Figs. 2(a)–2(e) confirm the reentrant phase diagram: the kinks and changes of slope in magnetization follow the same curved shape as the anomalies in heat capacity. The derivative dM/dB shown in Fig. 2(e) underscores this observation. Second, the temperature-dependent magnetization data in Figs. 2(a)–2(c) and [(d), inset] clearly show the ferromagnetic (FM) nature of the low-temperature phase: at base temperature there is a spontaneous moment that vanishes above T_C. Ferromagnetism is also indicated by the characteristic field sweeps in panels (j)–(k). Note, however, the difference between the field-cooled and zero-field cooled magnetization in Fig. 2(c) at 0.02 T below the transition temperature, indicating some difference in field-cooled vs zero-field cooled magnetic order for low fields. For higher fields, [panels (a) and (b)], there is no visible difference between fc-fh and zfc-fh data. Third, the considerable hysteresis in temperature sweeps in Figs. 2(a)–2(c) confirms previous reports of a first-order phase transition in $Yb_2Ti_2O_7$ [26,28], which occurs discontinuously via nucleation and domain growth, causing significant hysteresis in the order parameter vs temperature. The first order nature is also confirmed by the spontaneous moment [Fig. 2(d), inset], computed from field-dependent magnetization (as described in the Supplemental Material [25]) having no temperature dependence below T_C. Fourth and finally, the field sweeps in Figs. 2(f)–2(k) show asymmetric minor hysteresis loops for temperatures between 0.3 and 0.4 K (where the field scan passes through the phase boundary twice). This hysteresis is an additional indication of the discontinuous first-order phase boundary.

The neutron diffraction measurements in Fig. 3 clearly show the onset of the magnetic order seen in the magnetization, and corroborate the reentrant phase diagram of $Yb_2Ti_2O_7$: the temperature scans in Figs. 3(b)–3(d) show transition temperatures (defined as the temperature where the Bragg intensity begins to increase) following the same field dependence as heat capacity and magnetization. Additionally, the data in Figs. 3(b)–3(d) confirm the first-order nature of the phase transition, with massive hysteresis in the temperature scans, even though the scans were extremely slow [the scans in panels (c) and (d) had sweep rates of 0.6 mK/min]. Note, however, that no hysteresis is apparent in the 100 mK field sweep of the $(2\bar{2}0)$ peak [Fig. 2(a)]. This suggests either a second order phase transition, or a weakly first order transition.

Closer examination of the $(2\bar{2}0)$ neutron diffraction provides more clues about the magnetic order. In particular,

FIG. 3.   Field and temperature dependence of the $(2\bar{2}0)$ Bragg peak intensity. (a) Magnetic field scan going up $(+B)$ and down $(-B)$ in field. Note the lack of hysteresis. (b)–(d) Temperature scans at external magnetic fields of 550, 300, and 0 mT (internal fields of 473, 239, and 0 mT). Red indicates increasing temperature, blue indicates decreasing temperature. Error bars indicate 1 standard deviation above and 1 standard deviation below the measured value.

TABLE I. Refinement to neutrons scattering intensities, allowing canting angle and ordered moment size to vary.

Structure	μ (μ_B)	θ	χ^2	χ^2_{domain}	μ_{fit} (μ_B)	θ_{fit}
Gaudet [11]	0.90(9)	14(5)°	85.5	11.66	0.90(3)	8(6)°
Yaouanc [14]	0.95(2)	26.3(6)°	85.8	18.13	0.851(2)	6.2(1)°

the field-dependent scattering in Fig. 3(a) is inconsistent with that of a kagome ice phase. We compared the $Yb_2Ti_2O_7$ data to the $(2\bar{2}0)$ scattering for $Ho_2Ti_2O_7$ entering the kagome ice phase [35], which has steplike increases in $(2\bar{2}0)$ intensity signaling entry and exit from the kagome-ice state. For $Yb_2Ti_2O_7$, the steady increase in scattering suggests that spins continuously cant from a ferromagnetic ordered state as field increases, until at 0.57 T they undergo a transition to a state polarized along $\langle 111 \rangle$, causing a drop in $(2\bar{2}0)$ intensity.

To determine the low T ordered spin state we collected difference data at $(2\bar{2}0)$, $(4\bar{4}0)$, and (311). We performed a refinement to the observed Bragg intensities using the structures reported by Gaudet *et al.* (two canted in, two canted out) [11] and Yaouanc *et al.* (all canted in all canted out) [14], allowing the canting angle and moment size to vary. More details are provided in the Supplemental Material [25]. The results are shown in Table I. Although our refinement contained only three peaks and did not account for extinction, some basic conclusions can be drawn. First, we found that fitting peak intensities to either structure requires the existence of ferromagnetic domains. Evidence for ferromagnetic domains was previously observed [28], and the presence of domains is consistent with the vanishing zero field magnetization in Figs. 2(f)–2(k). Second, our refined moment and angle are consistent with the Gaudet *et al.* structure, but not with the Yaouanc *et al.* structure. Given the limited data in our refinement, this should not be taken as conclusive, but as corroborating evidence for the two-in-two-out structure.

We can amalgamate the anomalies in heat capacity, magnetization, and neutron scattering to build a phase diagram of $Yb_2Ti_2O_7$ in a $\langle 111 \rangle$ oriented field, shown in Fig. 4(a). All measurements concur on the phase boundary's location. We double checked for consistency between the various data sets by computing ΔS using the Clapeyron equation for a first order phase boundary $(\Delta S/\Delta M) = -\mu_0(\partial H/\partial T)$, and then compared the result to ΔS computed from heat capacity, shown in Fig. 4(b). (See Supplemental Material [25] for more details.) The agreement corroborates the first-order nature of the phase boundary.

Three model spin Hamiltonians have been determined for $Yb_2Ti_2O_7$ by Ross *et al.* [4], Robert *et al.* [36], and Thompson *et al.* [12] through neutron scattering measurements, and we used these as the basis for classical Monte Carlo simulations. The specific heat and average magnetization along $\langle 111 \rangle$ were evaluated by measuring thermal averages employing up
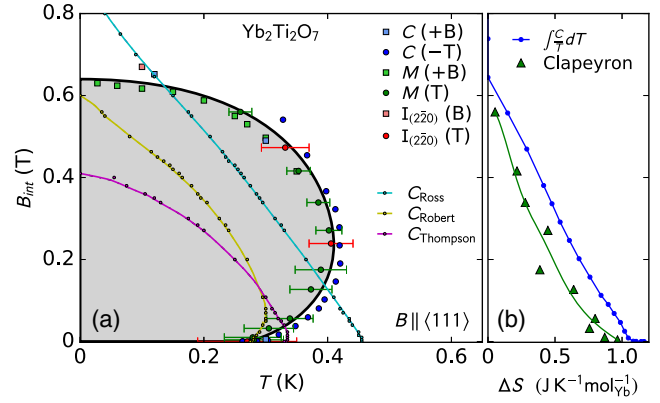

FIG. 4. (a) Phase diagram of $Yb_2Ti_2O_7$ in a $\langle 111 \rangle$ oriented field, built from heat capacity, magnetization, and neutron scattering. Heat capacity points denote peak location (see Fig. 1), magnetization points denote inflection points (see Fig. 2), and neutron scattering points denote where intensity begins increasing (see Fig. 3). Error bars indicate the difference in transition temperature upon heating vs cooling. Theoretically predicted phase boundaries are shown with the small data points that denote the location of simulated heat capacity peaks. The colored lines are guides to the eye. (b) Change in entropy (ΔS) extracted from heat capacity compared to ΔS computed from the Clapeyron relation. The green line is a guide to the eye.

to 4×10^5 samples per spin. The simulations were carried out on a pyrochlore lattice with $N = 4L^3$ spins and periodic boundary conditions. Here, L is the number of unit cells along each direction, which varied from 6 to 30 in our simulations. The results shown are for $L = 10$; other simulations confirmed that finite size effects were small away from phase boundaries. More details of the Monte Carlo calculations and results are provided in the Supplemental Material [25], which includes Ref. [37]. The overall field and temperature scale of the computed phase boundaries to FM order are in accord with the data, with the Robert *et al.* parameters coming the closest. The simulations also predict a first order phase boundary throughout. However, the marked lobelike shape of the phase diagram is not reproduced, except for a small bulge predicted by the Hamiltonian parameters of Robert *et al.* that is 5 times too small in temperature.

There are two obvious potential sources of the discrepancy. First, long-range magnetic dipolar interactions—not included in our simulation—may cause the spins to align more easily under a field. Alternatively, the enhancement of magnetic order in a small field may be interpreted as a suppression of magnetic order in zero field relative to the classical MC result. In other words, quantum fluctuations may suppress the zero-field ordering temperature. Various studies have predicted ground state quantum fluctuations from competition between ferromagnetic and antiferromagnetic phases [36,38,39]; the fact that the simulations using the Robert *et al.* Hamiltonian—which is near the FM-AFM boundary—comes the closest to the observed phase diagram may lend credence to this theory. Given the evidence

PHYSICAL REVIEW LETTERS

for monopoles in the paramagnetic phase [7,8], it is also worth noting that the noncollinear spin structure in the $Yb_2Ti_2O_7$ ordered phase (FM canted 2-in-2-out) does not preclude collective ground state quantum fluctuations: even though the order is ferromagnetic, the ice rule required for the QSI effective field theory is approximately preserved in the lattice. In that case, the pocket of phase space that opens up between the MC phase boundary and the observed phase boundary could be a finite temperature manifestation of a $U(1)$ quantum spin liquid. Such quantum fluctuations would lower the transition temperature and might persist in the zero-field ground state. Indeed, zero-field spin fluctuations in $Yb_2Ti_2O_7$ have been found to be extremely broad in energy [11]. This is inconsistent with conventional spin waves of the ordered state and points instead to remnant fractionalized excitations of a spin liquid regime.

In summary, we have used stoichiometric single crystals of $Yb_2Ti_2O_7$ to reveal a peculiar reentrant phase diagram in a $\langle 111 \rangle$ oriented field, which current model Hamiltonians cannot explain within a classical short range Monte Carlo simulation. The zero-field ordered state is ferromagnetic with domains, the spins seem to polarize along $\langle 111 \rangle$ above an internal field of 0.65 T, and magnetization hysteresis hints at a correlated domain structure. The peculiar decrease in ordering temperature for $\langle 111 \rangle$ fields below 0.2 T may be a first tangible indication of the proximity of $Yb_2Ti_2O_7$ to a quantum spin liquid phase.

[1] J. A. Hodges, P. Bonville, A. Forget, A. Yaouanc, P. Dalmas de Réotier, G. André, M. Rams, K. Królas, C. Ritter, P. C. M. Gubbens, C. T. Kaiser, P. J. C. King, and C. Baines, Phys. Rev. Lett. **88**, 077204 (2002).

[2] J. A. Hodges, P. Bonville, A. Forget, M. Rams, K. Krolas, and G. Dhalenne, J. Phys. Condens. Matter **13**, 9301 (2001).

[3] J. Gaudet, D. D. Maharaj, G. Sala, E. Kermarrec, K. A. Ross, H. A. Dabkowska, A. I. Kolesnikov, G. E. Granroth, and B. D. Gaulin, Phys. Rev. B **92**, 134420 (2015).

[4] K. A. Ross, L. Savary, B. D. Gaulin, and L. Balents, Phys. Rev. X **1**, 021002 (2011).

[5] N. R. Hayre, K. A. Ross, R. Applegate, T. Lin, R. R. P. Singh, B. D. Gaulin, and M. J. P. Gingras, Phys. Rev. B **87**, 184423 (2013).

[6] R. Applegate, N. R. Hayre, R. R. P. Singh, T. Lin, A. G. R. Day, and M. J. P. Gingras, Phys. Rev. Lett. **109**, 097205 (2012).

[7] L. Pan, N. J. Laurita, K. A. Ross, B. D. Gaulin, and N. P. Armitage, Nat. Phys. **12**, 361 (2016).

[8] Y. Tokiwa, T. Yamashita, M. Udagawa, S. Kittaka, T. Sakakibara, D. Terazawa, Y. Shimoyama, T. Terashima, Y. Yasui, T. Shibauchi, and Y. Matsuda, Nat. Commun. **7**, 10807 (2016).

[9] M. J. P. Gingras and P. A. McClarty, Rep. Prog. Phys. **77**, 056501 (2014).

[10] L. Balents, Nature (London) **464**, 199 (2010).

[11] J. Gaudet, K. A. Ross, E. Kermarrec, N. P. Butch, G. Ehlers, H. A. Dabkowska, and B. D. Gaulin, Phys. Rev. B **93**, 064406 (2016).

[12] J. D. Thompson, P. A. McClarty, D. Prabhakaran, I. Cabrera, T. Guidi, and R. Coldea, Phys. Rev. Lett. **119**, 057203 (2017).

[13] Y. Yasui, M. Soda, S. Iikubo, M. Ito, M. Sato, N. Hamaguchi, T. Matsushita, N. Wada, T. Takeuchi, N. Aso, and K. Kakurai, J. Phys. Soc. Jpn. **72**, 3014 (2003).

[14] A. Yaouanc, P. D. de Réotier, L. Keller, B. Roessli, and A. Forget, J. Phys. Condens. Matter **28**, 426002 (2016).

[15] E. Kermarrec, J. Gaudet, K. Fritsch, R. Khasanov, Z. Guguchia, C. Ritter, K. A. Ross, H. A. Dabkowska, and B. D. Gaulin, Nat. Commun. **8**, 14810 (2017).

[16] J. Carrasquilla, Z. Hao, and R. G. Melko, Nat. Commun. **6**, 7421 (2015).

[17] A. Yaouanc, P. Dalmas de Réotier, C. Marin, and V. Glazkov, Phys. Rev. B **84**, 172408 (2011).

[18] K. A. Ross, L. R. Yaraskavitch, M. Laver, J. S. Gardner, J. A. Quilliam, S. Meng, J. B. Kycia, D. K. Singh, T. Proffen, H. A. Dabkowska, and B. D. Gaulin, Phys. Rev. B **84**, 174442 (2011).

[19] K. A. Ross, T. Proffen, H. A. Dabkowska, J. A. Quilliam, L. R. Yaraskavitch, J. B. Kycia, and B. D. Gaulin, Phys. Rev. B **86**, 174424 (2012).

[20] R. M. D'Ortenzio, H. A. Dabkowska, S. R. Dunsiger, B. D. Gaulin, M. J. P. Gingras, T. Goko, J. B. Kycia, L. Liu, T. Medina, T. J. Munsie, D. Pomaranski, K. A. Ross, Y. J. Uemura, T. J. Williams, and G. M. Luke, Phys. Rev. B **88**, 134428 (2013).

[21] A. Mostaed, G. Balakrishnan, M. R. Lees, Y. Yasui, L.-J. Chang, and R. Beanland, Phys. Rev. B **95**, 094431 (2017).

[22] K. E. Arpino, B. A. Trump, A. O. Scheie, T. M. McQueen, and S. M. Koohpayeh, Phys. Rev. B **95**, 094407 (2017).

[23] Certain commercial instruments are identified in this Letter to foster understanding. Such identification does not imply recommendation or endorsement by the National Institute of Standards and Technology, nor does it imply that the instruments identified are necessarily the best available for the purpose.

[24] A. Scheie, arXiv:1705.07129.

[25] S. Legl, See Supplemental Material at http://link.aps.org/supplemental/10.1103/PhysRevLett.119.127201 for more details of the experimental and computational methods.

[26] Y. Yasui, N. Hamachi, Y. Kono, S. Kittaka, and T. Sakakibara, SPIN **05**, 1540002 (2015).

[27] E. Lhotel, S. R. Giblin, M. R. Lees, G. Balakrishnan, L. J. Chang, and Y. Yasui, Phys. Rev. B **89**, 224419 (2014).

[28] L.-J. Chang, S. Onoda, Y. Su, Y.-J. Kao, K.-D. Tsuei, Y. Yasui, K. Kakurai, and M. R. Lees, Nat. Commun. **3**, 992 (2012).

[29] A. Aharoni, J. Appl. Phys. **83**, 3432 (1998).

[30] S. Legl, C. Pfleiderer, and K. Krämer, Rev. Sci. Instrum. **81**, 043911 (2010).

[31] C. Krey, S. Legl, S. R. Dunsiger, M. Meven, J. S. Gardner, J. M. Roper, and C. Pfleiderer, Phys. Rev. Lett. **108**, 257204 (2012).

[32] S. Legl, C. Krey, S. R. Dunsiger, H. A. Dabkowska, J. A. Rodriguez, G. M. Luke, and C. Pfleiderer, Phys. Rev. Lett. **109**, 047201 (2012).

[33] S. Legl, Doktorarbeit Technische Universität München, 2010.

[34] A. Zheludev, Reslib 3.4c, (2009).

[35] T. Fennell, S. T. Bramwell, D. F. McMorrow, P. Manuel, and A. R. Wildes, Nat. Phys. **3**, 566 (2007).

[36] J. Robert, E. Lhotel, G. Remenyi, S. Sahling, I. Mirebeau, C. Decorse, B. Canals, and S. Petit, Phys. Rev. B **92**, 064425 (2015).

[37] J. Cardy, *Scaling and Renormalization in Statistical Physics* (Cambridge University Press, Cambridge, England, 1996).

[38] L. D. C. Jaubert, O. Benton, J. G. Rau, J. Oitmaa, R. R. P. Singh, N. Shannon, and M. J. P. Gingras, Phys. Rev. Lett. **115**, 267208 (2015).

[39] H. Yan, O. Benton, L. Jaubert, and N. Shannon, Phys. Rev. B **95**, 094422 (2017).